doi: 10.82124/CEAS-GNC-2026-058 CEAS-GNC-2026-058

A 3D Mixed-Integer Linear Optimization Problem for Bridge Inspection by a UAV Swarm with LOS Connectivity Constraints

Jean-Luc Sarvadon Ph.D. Student, Politecnico di Torino, Torino, Italy. jeanluc.sarvadon@polito.it

Pierantonio Bertuccio Ph.D. Student, Politecnico di Torino, Torino, Italy. pierantonio.bertuccio@polito.it

Petre Ricioppo Ph.D. Student, Politecnico di Torino, Torino, Italy. petre.ricioppo@polito.it

Giorgia Giacalone Research Fellow, Politecnico di Torino, Torino, Italy. giorgia.giacalone@polito.it

Riccardo Enrico Ph.D. Student, Politecnico di Torino, Torino, Italy. riccardo.enrico@polito.it

Fausto Francesco Lizzio Assistant Professor, Politecnico di Torino, Torino, Italy. fausto.lizzio@polito.it

ABSTRACT

In this paper, a motion planning mission is considered for a swarm of Unmanned Aerial Vehicles. In particular, a Mixed-Integer Linear Programming optimization problem is formulated to maximize the number of visited targets and minimize the total control effort, while avoiding obstacles and inter-agent collisions. A Line-Of-Sight constraint is enforced in the optimization procedure to ensure visibility-based inter-agent connectivity for the whole mission duration. Different from similar approaches in the literature, the present work extends the treatment to a 3D configuration and exploits a different graph topology constraint based on a multi-commodity flow model. This graph formulation allows more versatility in the feasible topologies. A bridge inspection mission is selected to frame the algorithm in a real-world scenario. The results show that the proposed algorithm consistently generates feasible multi-agent trajectories with steady connectivity, whereas the baseline approach may fail due to the stronger limitations in the graph formulation.

Keywords: mixed-integer optimization, UAV swarm, LOS constraint, bridge inspection

1 Introduction

In recent years, there has been a growing interest in Unmanned Aerial Vehicles (UAVs) technology due to their low instrumentation costs, compact size, and the ability to carry various payloads, [1]. Deploying unmanned drones reduces the risk for human resources or expensive technology, [2]. Recently, multi-agent missions have gained significant momentum, as cooperation among drones can lead to improved efficiency, reduced operational time, and robustness against a single point of failure, [3].

For these reasons, UAVs are now being integrated into different fields, including agriculture, environmental monitoring, search and rescue operations, and inspection [4]. In particular, through the integration of cameras, LiDAR, infrared, or ultrasonic sensors, infrastructure inspection has been widely

investigated, [5]. Indeed, the low efficiency and safety limitations of traditional assessments have driven the development of visual-based algorithms for UAVs, [6, 7].

In this kind of application, environmental features are generally known, and the mission can be planned offline. Hence, the problem can be framed into a motion planning optimization formulation. Various approaches have been explored in the literature to address this task while embedding several features of UAV-related missions. The work of [8] proposed a two-step optimization algorithm to determine viewpoints that ensure full coverage of a known target. Similarly, a 2D Mixed-Integer Linear Programming (MILP) solution was developed in [9], optimizing path coverage with the presence of obstacles. Additionally, in the work of [10], an MILP approach was formulated for path planning, incorporating inter-agent collision avoidance. Moreover, a fuel-constrained path-planning strategy was introduced in [11] for multiple vehicles in 2D using MILP, suggesting a potential extension to 3D scenarios.

Notably, a key issue in such applications is the loss of communication with the Ground Control Station (GCS), [12]. Indeed, UAV connectivity may be hindered by environmental obstacles and relies on a Line-Of-Sight (LOS) link for data transmission [13]. Several solutions to enforce such constraints for different objectives have been proposed in the literature. The work of [14] maximizes the amount of collected data from a single drone while ensuring LOS with fixed GCSs. In [15], the communication maintenance of ground robots' formation is studied through a polygonal decomposition of the environment. The optimal placement and orientation problem for multiple fixed UAVs in a LOS-constrained environment was studied in [16] through an integer linear programming.

When considering mobile agents, the swarm must maintain a LOS spanning tree that ensures connectivity to the GCS for the whole mission duration [17], [18]. Thus, the LOS constraint must be tightly coupled with both the topology constraint, ensuring that a spanning tree is present in the graph, and the connectivity constraint, ensuring that any two connected agents lie within their communication range. In the works of [19], [20], a MILP model in a 2D map is formulated, incorporating an LOS, a topology, and a connectivity constraint. However, the topology constraint described in [19], [20] only allowed for a connected graph whose diameter is less than or equal to two, [21]. Reminding that the diameter of a graph is the largest length of the path connecting two distinct vertices, this formulation greatly reduces the number of feasible topologies, especially for a high swarm cardinality.

In this paper, an MILP problem is introduced to optimize control efforts and maximize target coverage. The graph topology constraint is formulated through a multicommodity flow model, allowing a greater variability in the admitted topology by avoiding the limitation on the graph diameter, [22]. The algorithm ensures the maintenance of an LOS-based spanning tree without collisions between agents or with the surrounding obstacles. Moreover, the framework is extended to a 3D scenario.

This optimization approach can be applied to a wide range of multi-agent motion planning applications. We focus on bridge inspection to frame the proposed algorithm in a real-world scenario.

The paper is organized as follows. In Section 2, some preliminaries are given on the problem formulation and multi-agent systems. Section 3 outlines the optimization framework, describing the details of the 3D constraints. The simulation environment and the numerical results are provided in Section 4. Finally, conclusive remarks and comments on future works are given in Section 5.

In the following, the indexing notation $\mathcal{I}_a^b$ denotes the set of integers from a to b.

2 Preliminaries

Consider a Multi-Agent System (MAS) consisting of n_a double-integrator agents in a 3D environment. The discrete-time dynamics for agent i are defined as

$$x_i(k+1) = Ax_i(k) + Bu_i(k) + g \tag{1}$$

where the state vector $x_i(k) = [p_{x,i}(k), v_{x,i}(k), p_{y,i}(k), v_{y,i}(k), p_{z,i}(k), v_{z,i}(k)]^\top$ comprises the spatial positions and velocities at instant k, while

$$A = \begin{bmatrix} 1 & T_s & 0 & 0 & 0 & 0 \\ 0 & 1 & 0 & 0 & 0 & 0 \\ 0 & 0 & 1 & T_s & 0 & 0 \\ 0 & 0 & 0 & 1 & 0 & 0 \\ 0 & 0 & 0 & 0 & 1 & T_s \\ 0 & 0 & 0 & 0 & 0 & 1 \end{bmatrix}, \quad B = \begin{bmatrix} \frac{1}{2}T_s^2 & 0 & 0 \\ T_s & 0 & 0 \\ 0 & \frac{1}{2}T_s^2 & 0 \\ 0 & T_s & 0 \\ 0 & 0 & \frac{1}{2}T_s^2 \\ 0 & 0 & T_s \end{bmatrix}, \quad g = \begin{bmatrix} 0 \\ 0 \\ 0 \\ 0 \\ -\frac{1}{2}gT_s^2 \\ -gT_s \end{bmatrix} \tag{2}$$

where T_s is the sampling time. The gravity has been explicitly stated to take into account the 3D scenario. The spatial occupancy of agent i at time k, denoted as $\mathcal{R}_i(k)$, evolves via Minkowski summation:

$$\mathcal{R}_i(k) \triangleq x_i(k) \oplus \mathcal{R}_i, \tag{3}$$

where $\mathcal{R}_i \subset \mathbb{R}^3$, for $i \in \mathcal{I}_1^{n_a}$, defines the agent's reference geometry centered at the origin. A square polytope of appropriate dimension is chosen to represent $\mathcal{R}_i$.

Agents navigate a workspace containing n_o static obstacles, modelled as convex polytopes

$$\mathcal{O}_c \subset \mathbb{R}^3, \quad c \in \mathcal{I}_1^{n_o}. \tag{4}$$

The admissible workspace for agent i is characterized as

$$\mathcal{A}_i(k) = \mathcal{A} \setminus \left(\bigcup_{c=1}^{n_o} \mathcal{O}_c \cup \bigcup_{j=1 j\neq i}^{n_a} \mathcal{R}_j(k) \right) \sim \mathcal{R}_i, \quad i \in \mathcal{I}_1^{n_a}, \tag{5}$$

where $\mathcal{A} \subset \mathbb{R}^3$ denotes the global operational domain, and $\sim$ enforces geometric exclusion constraints.

The agents are interconnected through an undirected interaction graph $\mathcal{G}(k) = \{\mathcal{N}(k), \mathcal{E}(k)\}$, where $\mathcal{N}(k)$ denotes the set of vertices while $\mathcal{E}(k)$ denotes the set of edges. If agent j belongs to the neighbourhood $\mathcal{N}_i(k) \subseteq \mathcal{N}(k)$ of agent i at instant k, their relative distance is less than or equal to the communication range, which is assumed to be uniform across the swarm. In this case, the agents are said to be connected. The degree matrix associated with $\mathcal{G}(k)$ is $D(k) \in \mathbb{R}^{n_a \times n_a}$. The degree matrix is diagonal, and its $\{i,i\}$-th element is $\deg_i(k) = |\mathcal{N}_i(k)|$. The connectivity region of an agent i is represented by $C_i(k)$, and it is defined as a square polytope centered on the agent. The width of the polytope is determined according to the agents' communication range.

The connectivity is tightly coupled to the LOS, which could be disrupted by the presence of obstacles. The LOS between two agents i and j is defined starting from the convex combination of their positions, i.e.,

$$\mathcal{L}_{i,j}(k) = \left\{ \ell(k) \in \mathbb{R}^3 \;\middle|\; \ell(k) = \lambda x_i(k) + (1-\lambda)x_j(k),\ \forall \lambda \in [0,1] \right\}. \tag{6}$$

Agents i and j are in LOS connectivity if

$$\mathcal{L}_{i,j}(k) \cap O_c = \emptyset, \quad c \in \mathcal{I}_1^{n_o},$$

where O_c is defined in (4).

In this work, polytopes are formulated through the half-space representation. Consider a generic convex polytope with n_s sides

$$\mathcal{P} = \{x \in \mathbb{R}^3 \mid Px \leq q\}, \tag{7}$$

where $P \in \mathbb{R}^{n_s \times 3}$, $q \in \mathbb{R}^{n_s}$, while $x \in \mathbb{R}^3$ represents a point in the 3D space, e.g., the agent's position. Calling P^h the h^{th} row of P and q^h the the h^{th} element of q, each inequality $P^h x \leq q^h$ defines a half-space boundary where P^h is the outward-facing normal vector of the h-th face, and q^h is the signed distance from the origin to the face along P^h. Polytopes' inequalities can be expressed through the Big-M method inside an optimization framework. This is a standard modelling technique used to represent conditional constraints and logical implications. Denoting as $b \in \{0, 1\}$ a binary decision variable, the implication

$$b = 1 \quad \Longrightarrow \quad P^h x \leq q^h,$$

can be equivalently formulated as

$$P^h x \leq q^h + M(1 - b), \tag{8}$$

with $M \in \mathbb{R}$ chosen as sufficiently large positive constant. When $b = 1$, the inequality is active, while when $b = 0$, the right-hand side is relaxed by M and the constraint is inactive. The constant M should be chosen large enough to effectively deactivate constraints when needed, but not too large to avoid numerical instability. The Big-M formulation enables the encoding of obstacle and inter-agent collision avoidance, connectivity, and LOS constraints, as explained in the next Section.

3 Optimization Problem

The optimization problem is formulated as an MILP, which defines a linear objective function subject to linear constraints while having decision variables of both integer and continuous values. The optimization is defined as follows

$$\min \quad \gamma_u \sum_{k=0}^{N} \sum_{i=1}^{n_a} \|u_i(k)\|_1 + \gamma_v \sum_{k=0}^{N} \sum_{i=1}^{n_a} \|v_{z,i}(k)\|_1 - \gamma_t \sum_{k=0}^{N} \sum_{e=1}^{n_t} \sum_{i=1}^{n_a} b_{i,e}^{\text{tar}}(k), \tag{9a}$$

s.t.

$\forall i \in \mathcal{I}_1^{n_a},\ i < j \leq n_a,\ \forall c \in \mathcal{I}_1^{n_o},\ \forall e \in \mathcal{I}_1^{n_t},\ \forall k \in \mathcal{I}_0^{N},$

$$x_i(k+1) = Ax_i(k) + Bu_i(k) + g, \tag{9b}$$

$$x_i(k+1) \in \mathcal{X}_i, \tag{9c}$$

$$u_i(k) \in \mathcal{U}_i, \tag{9d}$$

$$x_i(k+1) \in \mathcal{A}_i(k+1), \tag{9e}$$

$$\sum_{k=0}^{N} \sum_{h=1}^{n_a} b_{h,e}^{\text{tar}}(k) \leq 1, \tag{9f}$$

$$b_{i,e}^{\text{tar}}(k+1) \implies ||v_i(k+1)||_1 < \bar{v}, \tag{9g}$$

$$b_{i,j}^{\text{con}}(k+1) \implies \mathcal{L}_{i,j}(k+1) \cap O_c = \emptyset, \tag{9h}$$

$$b_{i,j}^{\text{con}}(k+1) \implies x_i(k+1) \in C_j(k+1), \tag{9i}$$

$$\sum_{\{i,j\} \in \mathcal{E}(k)} b_{i,j}^{\text{con}}(k) = n_a - 1, \tag{9j}$$

$$\sum_{(i,r) \in \mathcal{E}(k)} f_{i,r}^{r}(k) - \sum_{(r,j) \in \mathcal{E}(k)} f_{r,j}^{r}(k) = 1, \qquad \forall r \in R, \tag{9k}$$

$$\sum_{(\alpha,j)\in\mathcal{E}(k)} f^r_{\alpha,j}(k) \;-\; \sum_{(i,\alpha)\in\mathcal{E}(k)} f^r_{i,\alpha}(k) \;=\; 1, \qquad \forall r \in R, \tag{9l}$$

$$\sum_{(i,v)\in\mathcal{E}(k)} f^r_{i,v}(k) \;-\; \sum_{(v,j)\in\mathcal{E}(k)} f^r_{v,j}(k) \;=\; 0, \qquad \forall v \in \mathcal{N}\setminus\{r,\alpha\},\ \forall r \in R, \tag{9m}$$

$$f^r_{i,j}(k) \geq 0, \qquad \forall r \in R. \tag{9n}$$

$$f^r_{i,j}(k) + f^{r'}_{j,i}(k) \;\leq\; b^{\text{con}}_{i,j}(k), \qquad \forall r, r' \in R. \tag{9o}$$

The cost function (9a) consists of three objectives, i.e., the minimization of the control effort, the minimization of vertical velocities, and the maximization of visited targets. The positive weights $\gamma_u > 0$, $\gamma_v > 0$, and $\gamma_t > 0$ balance the relative importance of these objectives. The minimization of the vertical velocities was adopted to dampen the vertical oscillations, having introduced the gravity in the agents' dynamics. The integer decision variables are $b^{\text{tar}}_{i,e}(k)$ describe whether agent i visits target e at instant k.

The system constraints enforce agent dynamics through (9b), with state and input bounds specified by (9c) and (9d), respectively.

Obstacle and inter-agent collision avoidance are guaranteed by (9e), which confines agents to their designated operative regions defined in (5). Specifically, for obstacle avoidance of agent i, an inequality as (8) is written for each side h of $\mathcal{O}_c$, with the additional constraint

$$\sum_{h=1}^{n_s} b^{obs}_{i,c,h}(k) \geq 1$$

ensuring that at least one inequality is active without the Big-M relaxation. Similarly, for inter-agent collision avoidance of agent i, an inequality as (8) is written for each side h of $\mathcal{R}_j(k)$, with the additional constraint

$$\sum_{h=1}^{n_s} b^{col}_{i,j,h}(k) \geq 1.$$

Constraint (9f) prevents multiple visits to the same target. Additionally, given a polytope $\mathcal{T}_e$ with $e \in \mathcal{I}_1^{n_t}$ representing a target, an inequality as (8) is active if the variable $b^{\text{tar}}_{h,e}(k) = 1$ from some agent $h \in \mathcal{I}_1^{n_a}$.

Constraint (9g) enforces a speed limitation when the UAV is close to a target. Specifically, when $b^{\text{tar}}_{i,e}(k+1) = 1$, the velocity's norm-1 of agent i is constrained to be below a threshold $\bar{v}$. This models the requirement that, near a target, the drone should slow down to perform accurate sensing or data acquisition tasks at low speed.

Constraint (9h) enforces LOS by discretizing the segment $\mathcal{L}_{i,j}(k)$ defined in (6) into n_p intermediate points. For each obstacle $\mathcal{O}_c$, and for each point $p \in \mathcal{I}_1^{n_p}$, a pair of inequalities of the form (8) is introduced to determine whether the point lies in the intersection of two adjacent half-spaces defined by the obstacle. The additional constraint

$$\sum_{p=1}^{n_p} b^{LOS}_{i,j,c,p}(k) \;\geq\; 1 \tag{10}$$

ensures that at least one discretization point belongs to such an intersection, enforcing LOS. Only pairs of adjacent half-spaces are considered, since if agents i and j occupy non-adjacent half-spaces of an obstacle, the connecting segment $\mathcal{L}_{i,j}(k)$ is necessarily blocked, and LOS can not hold.

Through (9i), connected agents are enforced to lie inside their relative communication range. In particular, given a polytope C_i with $i \in \mathcal{I}_1^{n_a}$ defining the communication range, an inequality as (8) is active if the variable $b_{i,j}^{con}(k) = 1$ from some agent $j \in \mathcal{I}_1^{n_a}$.

The coupling between the LOS and the connectivity is ensured by

$$b_{i,j}^{con}(k) \leq \sum_{p=1}^{n_p} b_{i,j,c,p}^{LOS}(k). \tag{11}$$

Indeed, when no LOS is present between i and j, the $b_{i,j}^{con}(k)$ is enforced to be equal to zero. Instead, when agents i and j are in LOS, $b_{i,j}^{con}(k)$ can be either zero or one. Further details on this implementation can be found in [19, 20].

Constraints (9j)–(9o) enforce the multi-commodity flow balance, as formulated in [22]. Specifically, (9j) limits the number of edges to $n_a - 1$, avoiding cycles in the topology and ensuring that the resulting topology is actually a tree. Now, define a root node $\alpha \in \mathcal{N}$, a set of commodities $r \in R := \mathcal{N} \setminus \{\alpha\}$, and the flow of commodity $f_{i,j}^r(k) \geq 0$ on directed arc (i, j) at time k. Note that the selection of the root node is arbitrary. Constraint (9k) ensures that each destination $r \in R$ receives exactly one unit of its own commodity from the root node, while (9l) guarantees that the root node α supplies one unit of each commodity. Flow conservation at intermediate nodes is imposed by (9m), so that flow can only transit through such nodes without being generated or absorbed. Non-negativity of the flow variables is stated in (9n). Finally, the coupling constraint (9o) links the flow variables to the binary connectivity variables $b_{i,j}^{\text{con}}(k)$, ensuring that flow can be routed across an undirected edge $\{i, j\} \in \mathcal{E}(k)$ only if it is selected in the previous connectivity constraints.

4 Simulation Results

In this section, the simulation results are presented to show the effectiveness of the proposed method compared to the baseline approach in [20]. As mentioned in the introduction, the graph topology constraint in [20] generates connected graphs whose diameter must satisfy $\text{diam}(\mathcal{G}(k)) < 2$. Moreover, the formulation in [20] does not include constraint (9j), which limits the number of edges to $n_a - 1$. This allows for the presence of unnecessary cycles in the topology, requiring more communication links than needed. From a computational point of view, a higher number of edges also increases the number of LOS checks and related constraints that must be verified, leading to additional computational effort and time.

A swarm of $n_a = 5$ agents is selected to operate in a 3D environment map comprising a bridge. The agents are required to start the mission in the vicinity of a fixed control station and visit the highest number of targets. The agents are homogeneous double-integrators described in (1) and (2), with $T_s = 1$ s. The communication range is set to 30 m. The whole mission lasts $N = 30$ s. The bounds on the state and input vectors in the x-axis are $|p_{x,i}(k)| \leq 12.5$ m, $|v_{x,i}(k)| \leq 4$ m/s, and $|u_{x,i}(k)| \leq 1$ m/s^2 for $i = 2, \ldots, n_a$. The bounds on the state and input vectors in the y-axis are $|p_{y,i}(k)| \leq 27$ m, $|v_{y,i}(k)| \leq 4$ m/s, and $|u_{y,i}(k)| \leq 1$ m/s^2 for $i = 2, \ldots, n_a$. The bounds on the state and input vectors in the z-axis are $0\text{m} \leq p_{z,i}(k) \leq 22$ m, $|v_{z,i}(k)| \leq 4$ m/s, and $|u_{z,i}(k)| \leq 1$ m/s^2 for $i = 2, \ldots, n_a$. The velocity bound near the targets is set to $\bar{v} = 0.3$ m/s. The agent $i = 1$ is considered static to represent a fixed control station, so that its velocity and input bounds are set to zero along the three axes. The bridge consists of three pillars and a base, for a total of $n_o = 4$ parallelepiped obstacles with $n_s = 6$ sides. Each pillar displays one target on both sides, for a total of $n_t = 6$ targets. The segments $\mathcal{L}_{i,j}(k)$ describing the LOS constraints are divided into $n_p = 9$ intermediate points. The big-M variable is set to $M = 100$, while the weights in the cost function are $\gamma_u = 1$, $\gamma_v = 10$, and $\gamma_t = 1000$.

The simulations were performed in a computer equipped with an Intel® Core(TM) i7-14700HX CPU and 16 GB of RAM. The Gurobi® solver (version 12.0.1) was employed to solve the MILP. Three simulation runs are carried out.

In the first run, the solver is left free to choose the final positions of the non-fixed agents, as they are not assigned a priori. Figure 1 shows that the proposed algorithm generates the swarm trajectories visiting four targets while maintaining LOS-based graph connectivity and avoiding obstacles and inter-agent collisions. As it is possible to notice, the solver keeps agent $i = 3$ fixed, deeming it more convenient for minimizing the functional (9a) to only move three agents in total. The snapshots in Figures 2 show the LOS-based spanning tree at different time instants. The snapshot at time step $k = 30$ shows that the multi-commodity flow formulation generates a spanning tree whose $\text{diam}(\mathcal{G}(k)) = 3 > 2$, which would not be attainable through the algorithm in [20].

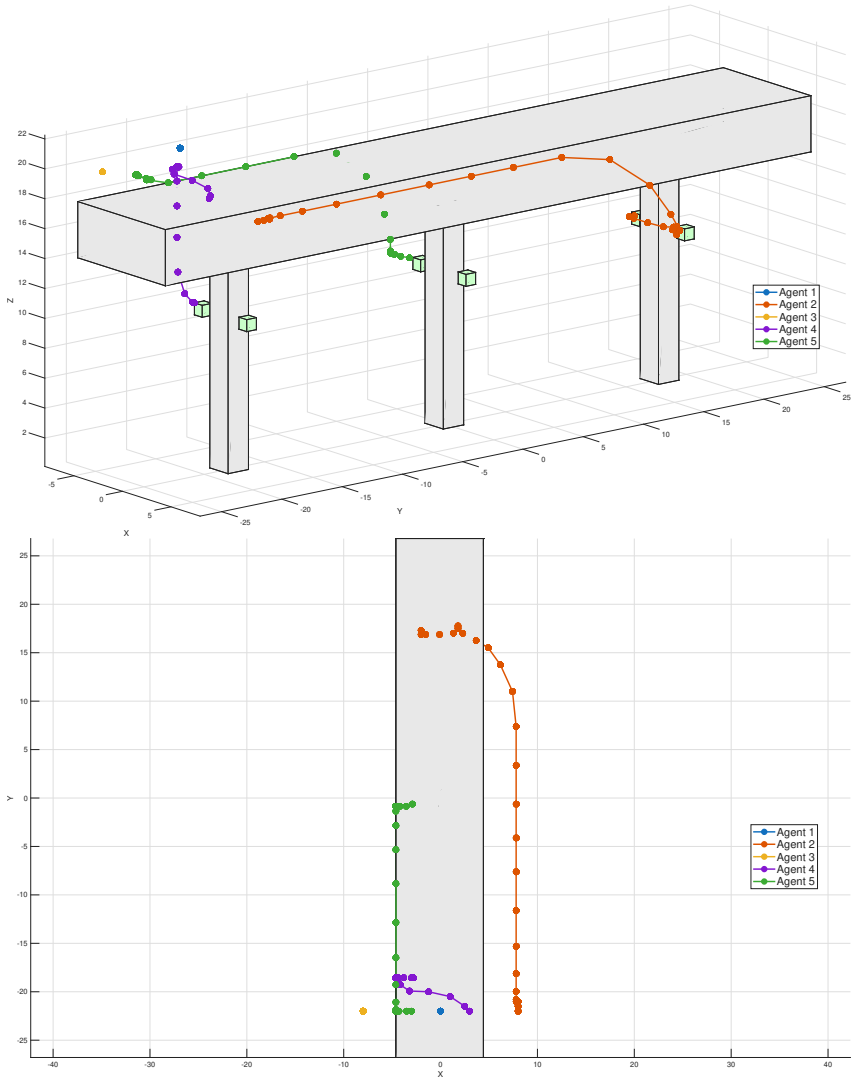

Fig. 1 Proposed approach: trajectories of the first simulation run.

The trajectories of the baseline approach in [20] are depicted in Figure 3 for the first simulation run. As the graph diameter must satisfy $\text{diam}(\mathcal{G}(k)) \leq 2$, the agents tend to cluster on one side of the bridge, thus visiting only three targets in total. The snapshots in Figures 4 show that the resulting topology contains unnecessary cycles in all the selected time instants.

In the second run, the solver is left free to choose the final positions for agents $i = 2, 3$, while the final positions of agents $i = 4, 5$ are assigned in the vicinity of the furthest pillar. Figure 5 shows that the algorithm generates the swarm trajectories visiting all the targets while maintaining LOS-based graph

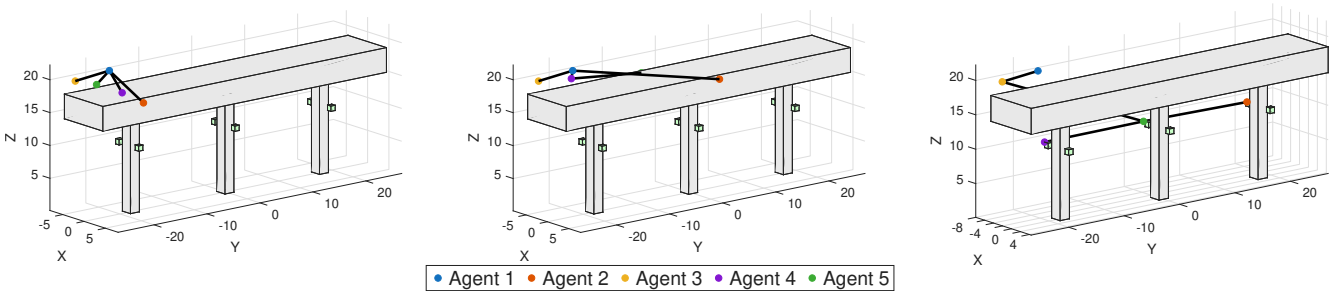

Fig. 2 Proposed approach: LOS-based connectivity of the first simulation at time instant $k = 1, 15, 30$.

connectivity and avoiding obstacles and inter-agent collisions. As it is possible to notice, the solver keeps agent 3 fixed again. The snapshots in Figures 6 show the LOS-based spanning tree at different time instants. The snapshots at time step $k = 15$ displays a spanning tree whose $\text{diam}(\mathcal{G}(k)) = 4 > 2$, while the snapshots at time step $k = 30$ displays a spanning tree whose $\text{diam}(\mathcal{G}(k)) = 3 > 2$.

The trajectories of the baseline approach in [20] are depicted in Figure 7 for the second simulation run. Again, the agents tend to cluster on one side of the bridge due to the graph diameter requirement. Thus, the swarm visits five targets in total. The snapshots in Figures 4 highlight the presence of unnecessary cycles in the resulting topology for all the selected time instants.

In the third run, the final positions are also assigned to agents $i = 2, 3$ at the centre of the bridge's base. Figure 9 shows that the algorithm generates the swarm trajectories visiting all the targets while maintaining LOS-based graph connectivity and avoiding obstacles and inter-agent collisions. The snapshots in Figures 10 show the LOS-based spanning tree at different time instants. The snapshots at time step $k = 15, 30$ display a spanning tree whose $\text{diam}(\mathcal{G}(k)) = 4 > 2$. For this peculiar configuration, the baseline approach in [20] could not provide a feasible solution. Indeed, the final positions assigned to the agents force the solver to split the swarm into two branches. However, the graph requirement $\text{diam}(\mathcal{G}(k)) \leq 2$ does not allow this, even for such a small cardinality $n_a = 5$.

Note that all the simulation runs comprise 17980 binary and 5240 continuous variables, and were given a total of 600s for the optimization. As this is an offline procedure, the computational time is not the main focus, and will be handled in future works as outlined in the next Section. Rather, the main highlight of this paper is the satisfaction of the LOS-based connectivity constraint in a challenging 3D scenario.

5 Conclusions

In this paper, a bridge inspection problem by a multi-agent system was developed through an MILP framework, taking into account LOS connectivity in a 3D scenario. Different from similar approaches found in the literature, a multi-commodity flow formulation was employed to constrain the interaction graph, allowing for a greater variability of the feasible topologies. The proposed algorithm was able to correctly design the agents' trajectories, while avoiding collisions and maximizing the number of visited targets. The comparison with a baseline approach limiting the graph diameter showed how heavily the topology constraint influences the mission outcome. As a next step, the resulting trajectories will be implemented in a realistic simulation scenario using ROS2/Gazebo. Moreover, an alternative obstacle avoidance formulation will be explored to reduce the computational time.

Declaration of Use of Artificial Intelligence

Artificial intelligence was not used in the work presented.

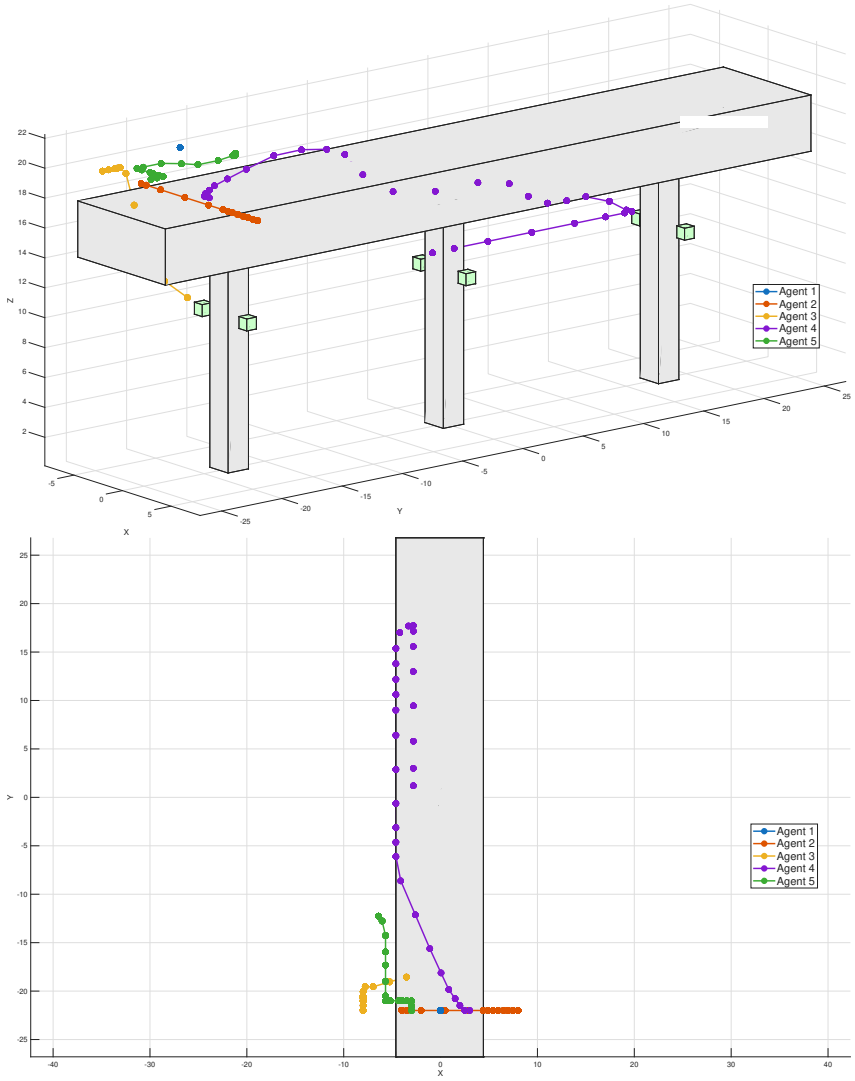

Fig. 3 Baseline approach: trajectories of the first simulation run.

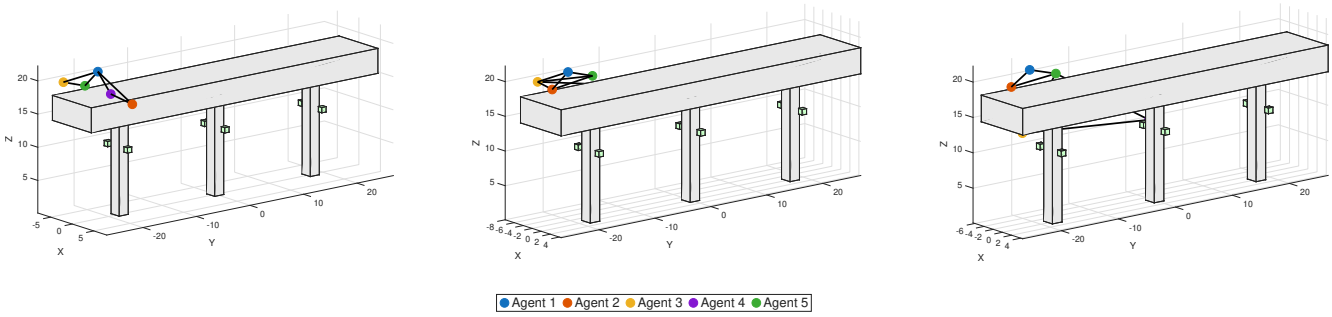

Fig. 4 Baseline approach: LOS-based connectivity of the first simulation at time instant $k = 1, 15, 30$.

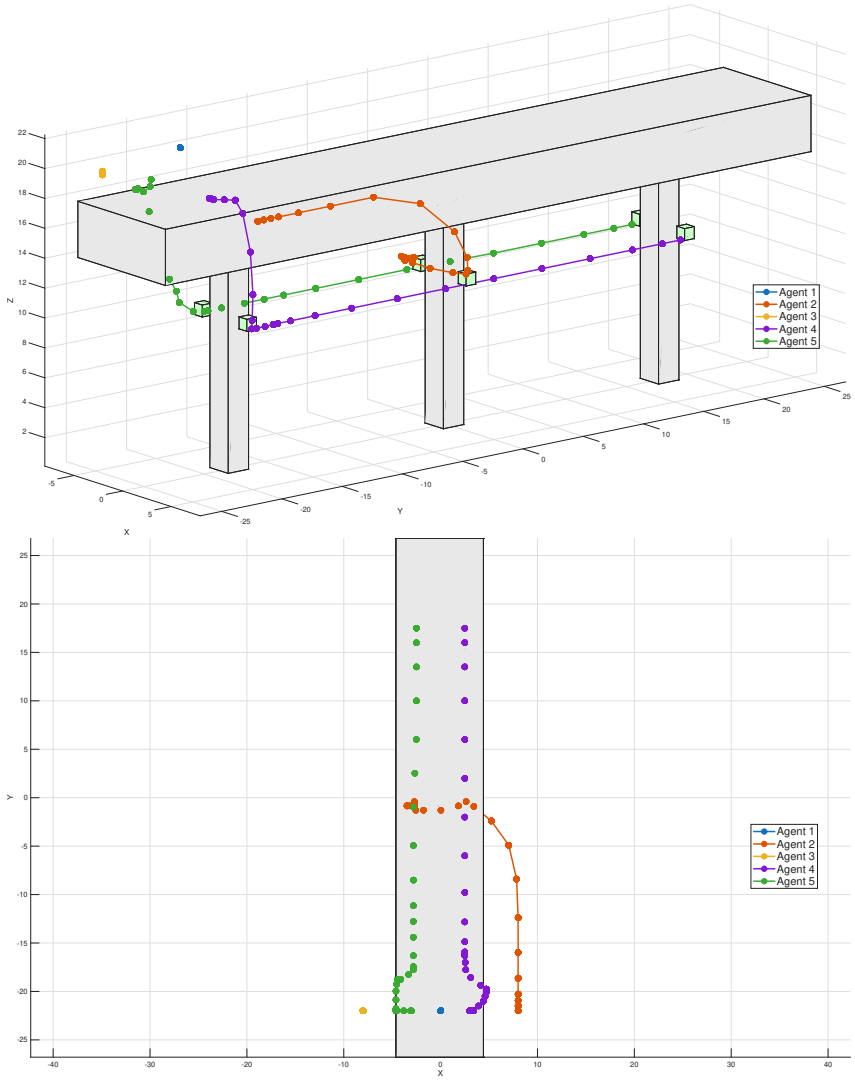

Fig. 5 Proposed approach: trajectories of the second simulation run.

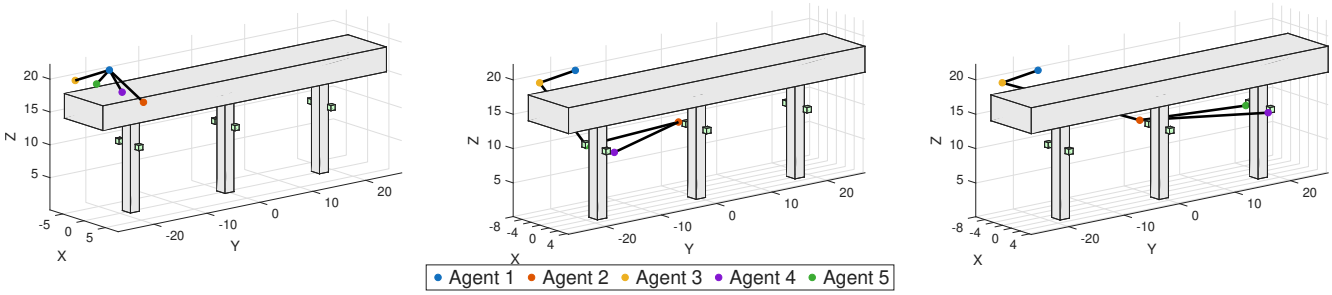

Fig. 6 Proposed approach: LOS-based connectivity of the second simulation at time instant $k = 1, 15, 30$.

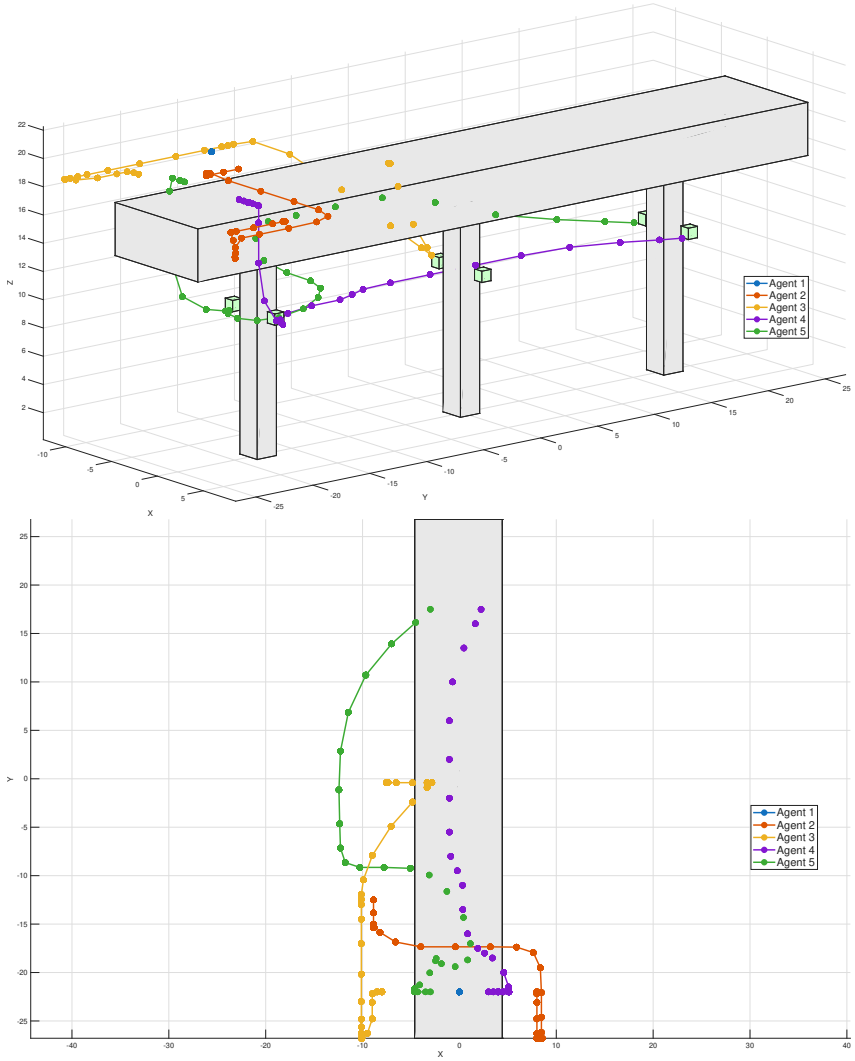

Fig. 7 Baseline approach: trajectories of the second simulation run.

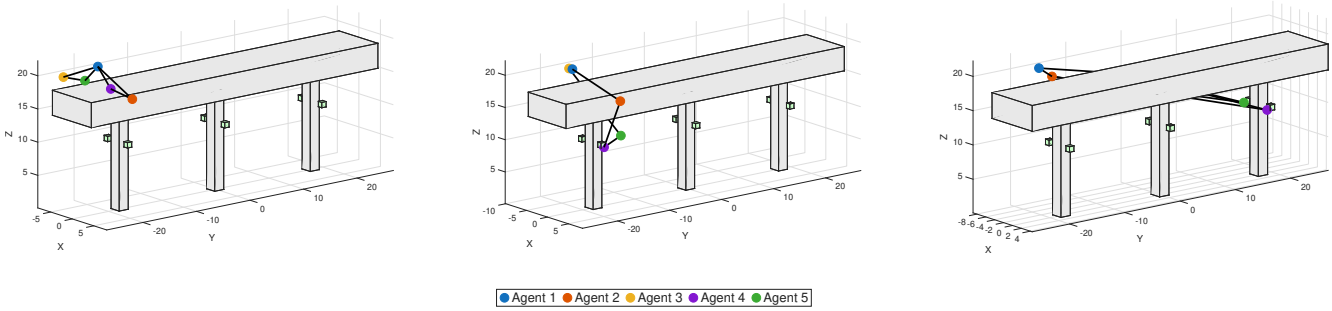

Fig. 8 Baseline approach: LOS-based connectivity of the second simulation at time instant $k = 1, 15, 30$.

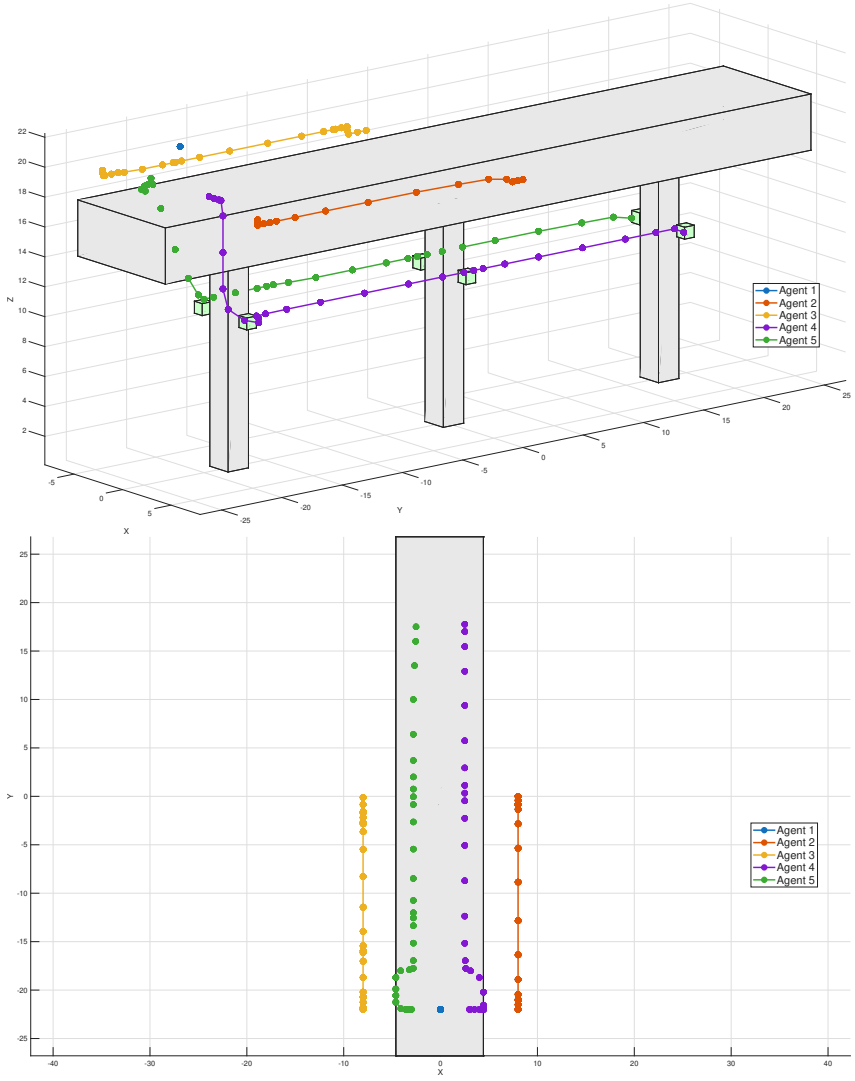

Fig. 9 Proposed approach: trajectories of the third simulation run.

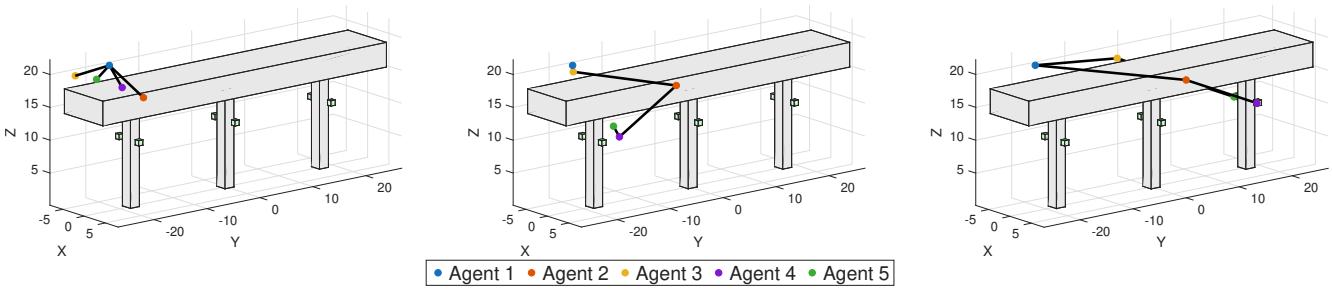

Fig. 10 Proposed approach: LOS-based connectivity of third simulation at time instant $k = 1, 15, 30$.

Fig. 11 This publication is part of the project PNRR-NGEU which has received funding from the MUR – DM 117/2023 and DM 630/2024 .

References

[1] Fazal Noor, Muhammad Asghar Khan, Ali Al-Zahrani, Insaf Ullah, and Kawther A. Al-Dhlan. A review on communications perspective of flying Ad-Hoc networks: Key enabling wireless technologies, applications, challenges and open research topics. *Drones*, 4(4), 2020. ISSN: 2504-446X. doi: 10.3390/drones4040065.

[2] Arnau Rovira-Sugranes, Abolfazl Razi, Fatemeh Afghah, and Jacob Chakareski. A review of AI-enabled routing protocols for UAV networks: Trends, challenges, and future outlook. *Ad Hoc Networks*, 130:102790, 2022. ISSN: 1570-8705. doi: https://doi.org/10.1016/j.adhoc.2022.102790.

[3] Fausto Francesco Lizzio, Elisa Capello, and Giorgio Guglieri. A review of consensus-based multi-agent UAV implementations. *Journal of Intelligent & Robotic Systems*, 106(43), 2022. doi: https://doi.org/10.1007/s10846-022-01743-9.

[4] Mohsan Syed Agha Hassnain, Othman Nawaf Qasem Hamood, Li Yanlong, Alsharif Mohammed H, and Khan Muhammad Asghar. Unmanned aerial vehicles (UAVs): practical aspects, applications, open challenges, security issues, and future trends. *Intelligent Services Robotics*, 16, 2023. ISSN: 1861-2784. doi: https://doi.org/10.1007/s11370-022-00452-4.

[5] Stefan Ivić, Bojan Crnković, Luka Grbčić, and Lea Matleković. Multi-UAV trajectory planning for 3D visual inspection of complex structures. *Automation in Construction*, 147:104709, 2023. ISSN: 0926-5805. doi: https://doi.org/10.1016/j.autcon.2022.104709.

[6] Kui Luo, Xuan Kong, Jie Zhang, Jiexuan Hu, Jinzhao Li, and Hao Tang. Computer vision-based bridge inspection and monitoring: A review. *Sensors*, 23(18), 2023. ISSN: 1424-8220. doi: 10.3390/s23187863.

[7] Yu-Fei Liu, Xin Nie, Jian-Sheng Fan, and Xiao-Gang Liu. Image-based crack assessment of bridge piers using unmanned aerial vehicles and three-dimensional scene reconstruction. *Computer-Aided Civil and Infrastructure Engineering*, 35(5):511–529, 2020. doi: https://doi.org/10.1111/mice.12501.

[8] A.Bircher, M.Kamel, K. Alexis, M. Burri, P. Oettershagen, S. Omari, T. Mantel, and R. Siegwart. Three-dimensional coverage path planning via viewpoint resampling and tour optimization for aerial robots. *Autonomous Robots*, 40, 2016. doi: 10.1007/s10514-015-9517-1.

[9] Wenxin Le, Zhentao Xue, Jian Chen, and Zichao Zhang. Coverage path planning based on the optimization strategy of multiple solar powered unmanned aerial vehicles. *Drones*, 6(8), 2022. ISSN: 2504-446X. doi: 10.3390/drones6080203.

[10] Arthur Richards and Jonathan P. How. Aircraft trajectory planning with collision avoidance using mixed integer linear programming. *Proceedings of the American Control Conference*, 3:1936 – 1941, 2002. doi: 10.1109/acc.2002.1023918.

[11] Tom Schouwenaars, Bart De Moor, Eric Feron, and Jonathan How. Mixed integer programming for multi-vehicle path planning. In *2001 European Control Conference (ECC)*, pages 2603–2608, 2001. doi: 10.23919/ECC.2001.7076321.

[12] Mohammad Mozaffari, Walid Saad, Mehdi Bennis, Young-Han Nam, and Mérouane Debbah. A tutorial on UAVs for wireless networks: Applications, challenges, and open problems. *IEEE Communications Surveys & Tutorials*, 21(3):2334–2360, 2019. doi: 10.1109/COMST.2019.2902862.

[13] Eran Greenberg, Amitay Bar, and Edmund Klodzh. LOS classification of UAV-to-ground links in built-up areas. In *2019 IEEE International Conference on Microwaves, Antennas, Communications and Electronic Systems (COMCAS)*, pages 1–5, 2019. doi: 10.1109/COMCAS44984.2019.8958045.

[14] Anqi Meng, Xiaozheng Gao, Yao Zhao, and Zhanxin Yang. Three-dimensional trajectory optimization for energy-constrained UAV-enabled iot system in probabilistic LoS channel. *IEEE Internet of Things Journal*, 9(2):1109–1121, 2022. doi: 10.1109/JIOT.2021.3079363.

[15] Ethan Stump, Nathan Michael, Vijay Kumar, and Volkan Isler. Visibility-based deployment of robot formations for communication maintenance. In *2011 IEEE International Conference on Robotics and Automation*, pages 4498–4505, 2011. doi: 10.1109/ICRA.2011.5980179.

[16] Javad Sabzehali, Vijay K. Shah, Harpreet S. Dhillon, and Jeffrey H. Reed. 3D placement and orientation of mmWave-based UAVs for guaranteed los coverage. *IEEE Wireless Communications Letters*, 10(8):1662–1666, 2021. doi: 10.1109/LWC.2021.3076463.

[17] Arun K. Majumdar. Chapter 4 - Fundamentals of free-space optical communications systems, optical channels, characterization, and network/access technology. In Arun K. Majumdar, editor, *Optical Wireless Communications for Broadband Global Internet Connectivity*, pages 55–116. Elsevier, 2019. ISBN: 978-0-12-813365-1. doi: https://doi.org/10.1016/B978-0-12-813365-1.00004-7.

[18] Yong Zeng, Rui Zhang, and Teng Joon Lim. Wireless communications with unmanned aerial vehicles: opportunities and challenges. *IEEE Communications Magazine*, 54(5):36–42, 2016. doi: 10.1109/MCOM.2016.7470933.

[19] Angelo Caregnato-Neto, Marcos R.O.A. Maximo, and Rubens J.M. Afonso. A line of sight constraint based on intermediary points for connectivity maintenance of multiagent systems using mixed-integer programming. *European Journal of Control*, 68:100671, 2022. ISSN: 0947-3580. 2022 European Control Conference Special Issue. doi: https://doi.org/10.1016/j.ejcon.2022.100671.

[20] Angelo Caregnato-Neto, Marcos R. O. A. Maximo, and Rubens J. M. Afonso. A novel line of sight constraint for mixed-integer programming models with applications to multi-agent motion planning. In *2023 European Control Conference (ECC)*, pages 1–6, 2023. doi: 10.23919/ECC57647.2023.10178275.

[21] G. Chartrand and P. Zhang. *A First Course in Graph Theory*. Dover books on mathematics. Dover Publications, 2012. ISBN: 9780486483689. doi: https://doi.org/10.1007/978-981-19-0957-3.

[22] Tamer F. Abdelmaguid. An efficient mixed integer linear programming model for the minimum spanning tree problem. *Mathematics*, 6(10), 2018. ISSN: 2227-7390. doi: 10.3390/math6100183.